Loss of Activities for mRNA Synthesis Accompanies Loss of λ2 Spikes from Reovirus Cores: An Effect of λ2 on λ1 Shell Structure

Cindy L. Luongo,*,†,[1] Xing Zhang,‡ Stephen B. Walker,‡ Ya Chen,§,[2] Teresa J. Broering,*,†,¶ Diane L. Farsetta,†,‖ Valorie D. Bowman,‡ Timothy S. Baker,‡ and Max L. Nibert*,†,¶,‖,[3]

*Department of Biochemistry, †Institute for Molecular Virology, §Integrated Microscopy Resource, and ‖Program in Cellular and Molecular Biology, University of Wisconsin–Madison, Madison, Wisconsin 53706; ‡Department of Biological Sciences, Purdue University, West Lafayette, Indiana 47907; and ¶Department of Microbiology and Molecular Genetics, Harvard Medical School, Boston, Massachusetts 02115

The 144-kDa λ2 protein, a component of the transcriptionally active reovirus core particle, catalyzes the last three enzymatic activities for formation of the 5′ cap 1 structure on the viral plus-strand transcripts. Limited evidence suggests it may also play a role in transcription per se. Particle-associated λ2 forms pentameric turrets ("spikes") around the fivefold axes of the icosahedral core. To address the requirements for λ2 in core functions other than the known functions in RNA capping, particles depleted of λ2 were generated from cores in vitro by a series of treatments involving heat, protease, and ionic detergent. The resulting particles contained less than 5% of pretreatment levels of λ2 but showed negligible loss of the other four core proteins or the 10 double-stranded RNA genome segments. Transmission cryo-electron microscopy (cryo-TEM) and scanning cryo-electron microscopy demonstrated loss of the λ2 spikes from these otherwise intact particles. In functional analyses, the "spikeless cores" showed greatly reduced activities not only for RNA capping but also for transcription and nucleoside triphosphate hydrolysis, suggesting enzymatic or structural roles for λ2 in all these activities. Comparison of the core and spikeless core structures obtained by cryo-TEM and three-dimensional image reconstruction revealed changes in the λ1 core shell that accompany λ2 loss, most notably the elimination of small pores that span the shell near the icosahedral fivefold axes. Changes in the shell may explain the reductions in transcriptase-related activities by spikeless cores.   © 2002 Elsevier Science (USA)

INTRODUCTION

Mammalian orthoreovirus (reovirus), a member of the family *Reoviridae,* replicates in the cytoplasm of its host cells. The icosahedrally symmetric core particle, which is an assembly intermediate (Fields *et al.,* 1971; Morgan and Zweerink, 1974) and partial uncoating product (Mayor and Jordan, 1968; Shatkin and Sipe, 1968; Smith *et al.,* 1969) of the intact virion, is composed of five proteins and 10 segments of genomic double-stranded RNA (dsRNA). The main core shell, which surrounds the genome, consists of 120 copies of the λ1 core protein in a $T = 1$ arrangement with two copies of λ1 per asymmetric unit (Reinisch *et al.,* 2000). The shell is stabilized by 150 nodule-like monomers of the σ2 core protein, which bind to the outer surface of λ1 and appear to serve a clamp-like function (Dryden *et al.,* 1993; Reinisch *et al.,*

2000; Xu *et al.,* 1993). Sixty copies of the λ2 core protein form 12 pentameric "spikes" that protrude around each of the icosahedral fivefold axes of the core (Dryden *et al.,* 1993; Reinisch *et al.,* 2000; White and Zweerink, 1976). Each of these λ2 pentamers binds to the outer surface of the λ1 shell and also makes contact with five adjacent copies of σ2 (Reinisch *et al.,* 2000). The λ3 and μ2 core proteins, which are present in 12 and 12 to 24 copies per core, respectively (Coombs, 1998), are thought to contribute to an inwardly projecting structure that is bound to the underside of the λ1 shell near each fivefold axis (Dryden *et al.,* 1998). Thus, although in solution λ2 can associate with both λ1 and λ3 (Starnes and Joklik, 1993), in the core λ2 interacts with λ1 and σ2 but appears not to interact with the more internally located λ3 and μ2 proteins (Dryden *et al.,* 1998; Reinisch *et al.,* 2000).

Reovirus cores contain all of the enzymes necessary to synthesize full-length plus-strand RNA copies from each of the 10 dsRNA genome segments and to add a eukaryotic cap 1 structure ($^{m7N}GpppG^{m2′O}$) to the 5′ ends of those transcripts (Shatkin and Kozak, 1983). The transcripts are not 3′-polyadenylylated. The λ3 protein is the reovirus RNA-dependent RNA polymerase (Morozov, 1989; Starnes and Joklik, 1993), and the λ1 protein exhibits a nucleoside triphosphate phosphohydrolase (NTPase)/helicase activity that may be responsible for

---

[1] Present address: Department of Microbiology, University of Alabama–Birmingham, Birmingham, AL 35294.

[2] Present address: Electron Microscopy Facility, University of Minnesota Medical School, Minneapolis, MN 55455.

[3] To whom correspondence and reprint requests should be addressed at Department of Microbiology and Molecular Genetics, Harvard Medical School, 200 Longwood Avenue, Boston, MA 02115. Fax: (617) 738-7664. E-mail: mnibert@hms.harvard.edu.

24

unwinding or reannealing dsRNA during RNA synthesis (Bisaillon *et al.,* 1997; Noble and Nibert, 1997a). The λ1 protein also exhibits an RNA 5′ triphosphate phosphohydrolase (triphosphatase) activity (Bisaillon and Lemay, 1997). This enzymatic activity represents the first step in RNA capping, which yields a 5′-diphosphorylated plus-strand RNA as substrate for the capping RNA guanylyltransferase (GTase) (Furuichi *et al.,* 1976) (see next paragraph). Genetic analysis has indicated that μ2 also influences the NTPase activity of cores (Noble and Nibert, 1997b), but its specific role in transcription or capping remains unknown. The inwardly projecting structures which underlie the λ2 spikes in cores and are thought to be composed of λ3, μ2, and an N-terminal region of λ1 have been proposed to constitute the enzyme complexes that mediate both plus-strand RNA synthesis and the capping RNA 5′ triphosphatase activity (Dryden *et al.,* 1998). These complexes may also mediate the minus-strand replicase activity that generates the genomic dsRNA segments from plus-strand templates during reovirus assembly.

The λ2 protein in reovirus cores, which contains 1289 amino acids and has a mass of 144 kDa, is implicated in catalyzing the last three reactions in viral plus-strand RNA capping. An N-terminal 42-kDa domain of λ2 is the RNA GTase, which adds a GMP moiety to the 5′ end of the nascent, diphosphorylated transcript (Cleveland *et al.,* 1986; Luongo *et al.,* 2000; Mao and Joklik, 1991; Reinisch *et al.,* 2000; Shatkin *et al.,* 1983). In addition, residues 434 to 691 and 804 to 1022 in λ2 encompass two independent, seven-stranded β-sheet structures that are strongly suggestive of methyltransferase domains (Reinisch *et al.,* 2000). These respective domains are hypothesized to mediate the nucleoside-7N- and nucleoside-2′O-methyltransferase activities in RNA capping and each has been shown within core crystals to bind *S*-adenosyl-L-homocysteine (Reinisch *et al.,* 2000), which is the by-product of methyl transfer from *S*-adenosyl-L-methionine (SAM) during capping (Furuichi *et al.,* 1976). In addition, mutagenesis experiments showed that residues 827 and 829 within the putative nucleoside-2′O-methyltransferase domain are necessary for SAM binding in an *in vitro* assay (Luongo *et al.,* 1998). A 24,000-M_r (24K) C-terminal region of λ2 is dispensable for capping (Luongo *et al.,* 1997) but can undergo a conformational rearrangement during the structural transition between virion and core particles (Dryden *et al.,* 1993). This rearrangement opens a channel that extends radially along the full length of the λ2 spike (Dryden *et al.,* 1993; Reinisch *et al.,* 2000) and may be necessary for release of the nascent capped transcripts (Bartlett *et al.,* 1974; Yeager *et al.,* 1996).

Previous work showed that exposure of reovirus cores to pH 11.8 caused selective loss of the λ2 spikes, accompanied by a large decrease in transcription activity (White and Zweerink, 1976). Whether this loss of activity resulted from λ2 removal or some other effect of the treatment was undetermined. Nevertheless, the correlation between loss of λ2 and decrease in transcription activity suggested that λ2 is essential for function of either the RNA polymerase or an accessory protein involved in transcription (White and Zweerink, 1976). To investigate the possible role of λ2 in transcription, we attempted to remove λ2 from cores by high pH treatment as in the previous study but were unsuccessful (M. L. Nibert, unpublished data). Efforts in another laboratory have demonstrated selective loss of the λ2 spikes upon exposure of cores to 65°C (K. M. Coombs, personal communication).

Particles that lack the 24K C-terminal portion of λ2 can be produced when cores of reovirus type 3 Dearing (T3D) are heated to 52°C and then digested with chymotrypsin (CHT) (Luongo *et al.,* 1997). Analysis of these heat-and-CHT-treated cores (HC-cores) showed that they retain a 120,000-M_r (120K) N-terminal cleavage product of λ2 and normal amounts of the other core proteins and the dsRNA genome. These HC-cores possess levels of transcription and RNA capping similar to those of untreated cores (Luongo *et al.,* 1997). Thus, heat treatment and subsequent proteolytic removal of the 24K C-terminal region of λ2 do not inhibit core functions. Another new type of reovirus particle can be produced when virions are digested with CHT in the presence of the ionic detergents sodium dodecyl sulfate (SDS) or sodium tetradecyl sulfate (STS) (Chandran and Nibert, 1998). The particles obtained with STS remain fully infectious (Chandran and Nibert, 1998). Hence, this detergent treatment appears not to inhibit the particle-associated transcription and capping enzymes, whose functions are essential for infection. For the current study we hypothesized that, by adding STS to the protocol for generating HC-cores, we might cause additional conformational changes in the N-terminal portion of λ2, making it subject to selective degradation and providing a distinct approach to generate particles with reduced λ2 content. By obtaining and characterizing such λ2-deficient particles, we aimed to gain further information about the roles of λ2 in core structure and function.

RESULTS

Removal of λ2 protein from cores by treatments with heat, protease, and detergent

Purified cores were heated to temperatures between 52 and 60°C to induce conformational changes that render the C-terminal 24K portion of λ2 sensitive to proteolysis (Luongo *et al.,* 1997). Particles were then cooled and treated with CHT in the presence of STS. Analysis by SDS–polyacrylamide gel electrophoresis (SDS–PAGE) revealed that the band containing the three λ proteins had lower intensity than the same band obtained from untreated samples, consistent with the ex-
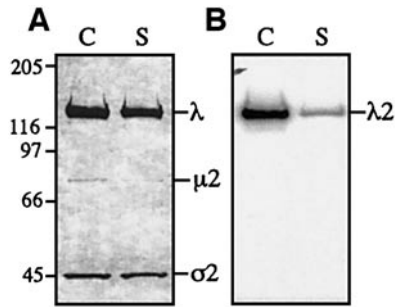
FIG. 1. Analysis of core particles treated with heat, CHT, and STS. Purified reovirus cores (C) or treated cores (S, for "spikeless") were analyzed for protein content (A) and $\lambda2$ autoguanylylation activity (B). Equivalent amounts of each particle type were resolved by SDS–PAGE. (A) Proteins were stained with Coomassie brilliant blue. The apparent molecular weights of protein standards ($\times10^{-3}$) are indicated at left. (B) Phosphorimager analysis was used to detect [^{32}P]GMP-labeled $\lambda2$ in the dried gel.

pected cleavage of $\lambda2$. The N-terminal 120K fragment of $\lambda2$ that is produced by heat-and-CHT treatment in the absence of detergent (Luongo *et al.,* 1997), however, was not seen on these gels. These results indicated that addition of STS to the treatment protocol permitted more complete degradation of $\lambda2$.

To determine which of the other core components remained particle-associated following the new treatment protocol, cores were heated to 52°C, cooled, and treated with CHT and STS. The particles were then purified by equilibrium centrifugation through a CsCl density gradient. A single, visually homogeneous particle band was isolated. Analysis of proteins by SDS–PAGE suggested that $\sigma2$, $\mu2$, and a majority of the λ proteins remained present in these particles (Fig. 1A). Immunoblot analyses showed that the levels of $\lambda1$ and $\lambda3$ remained similar to those in cores, whereas the amount of intact $\lambda2$ was greatly reduced (data not shown). Also, no $\lambda2$ cleavage fragments were detected (data not shown). Since the $\lambda2$ protein in cores can undergo autoguanylylation, whereby a single GMP moiety is covalently linked to a $\lambda2$ monomer (Cleveland *et al.,* 1986; Shatkin *et al.,* 1983), this activity was used to quantitate how much $\lambda2$ remained in the purified particles (Fig. 1B). Autoguanylylation followed by SDS–PAGE and phosphorimager analysis indicated that 13% ($\pm1.4\%$) of the amount of [α-^{32}P]GMP covalently bound to full-length $\lambda2$ in cores was found in the treated particles. This residual amount of full-length $\lambda2$ is similar to that remaining in HC-cores (18 $\pm$ 4.6%) (Luongo *et al.,* 1997). No $\lambda2$ cleavage products were visualized in the autoguanylylation assay (Fig. 1B), consistent with the more complete degradation of the cleaved $\lambda2$ molecules in the detergent-containing protocol.

Since the treatments with heat, CHT, and STS removed most of the $\lambda2$ protein from cores, we hypothesized that even greater removal might be achieved by purifying HC-cores before further treatment with these agents.

Particles generated with the sequential protocol formed a distinct band in a CsCl gradient at a density of 1.46 g/cm^3 (cores = 1.43 g/cm^3). Autoguanylylation followed by SDS–PAGE and phosphorimager analysis revealed these particles to contain only 3.6% ($\pm0.9\%$) of the amount of full-length $\lambda2$ in cores (Fig. 2A). No $\lambda2$ cleavage products were detected by immunoblot analysis (data not shown) or autoguanylylation analyses (Fig. 2A). Through other immunoblots, the particles were shown to contain approximately full levels of the other core proteins, including the transcriptase-associated proteins $\lambda3$ and $\mu2$ (Fig. 2B). In addition, these particles retained high levels of the 10 genomic dsRNA segments (Fig. 2C). From these experiments we concluded that the sequential treatment protocol is the one of choice for selective removal of $\lambda2$ from cores.

Transmission cryo-electron microscopy and three-dimensional image reconstruction of cores treated with heat, protease, and detergent show loss of $\lambda2$ spikes and subtle changes in the $\lambda1$ shell

To determine the structural effects of $\lambda2$ removal, cores and $\lambda2$-deficient cores generated by the sequential treatment protocol were embedded in vitreous ice and subjected to transmission cryo-electron microscopy (cryo-TEM) and three-dimensional (3-D) image reconstruction. Comparison of surface-shaded and cross-sectional representations of the 3-D reconstructions for cores and $\lambda2$-deficient cores showed the most striking
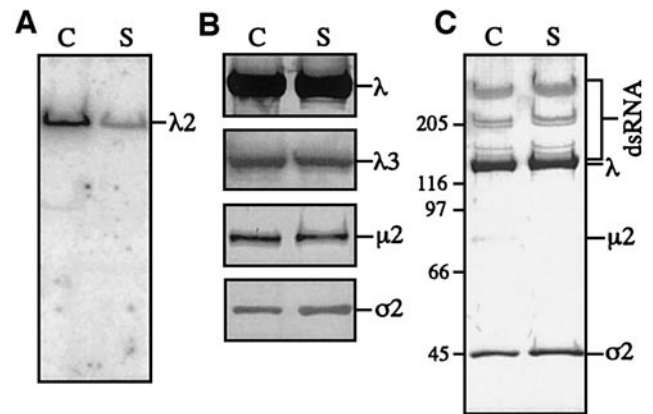

FIG. 2. Analysis of heat-and-CHT-treated cores (HC-cores) after further treatment with heat, CHT, and STS. Reovirus cores (C) or treated HC-cores (S, for spikeless) were analyzed for autoguanylylation activity (A), protein content (B), and dsRNA content (C). Equivalent amounts of each particle type were resolved by SDS–PAGE. (A) Phosphorimager analysis was used to detect [^{32}P]GMP-labeled $\lambda2$ in the dried gel. (B) Following transfer of sample pairs in duplicate to nitrocellulose, the membrane was divided into three equivalent strips, which were then probed with polyclonal anti-core, polyclonal anti-$\lambda3$, or polyclonal anti-$\mu2$ sera and visualized colorimetrically. The predominant reactivity of the anti-core serum is against the $\lambda1$, $\lambda2$, and $\sigma2$ proteins. (C) Proteins and dsRNA were stained, respectively, by sequential incubation with Coomassie brilliant blue and methylene blue.
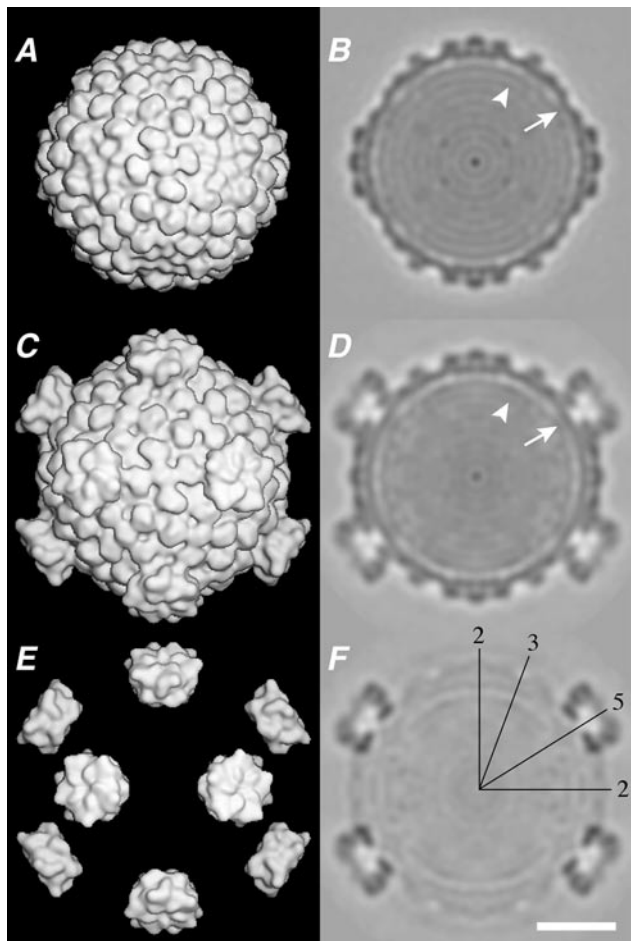
FIG. 3. Cryo-TEM and 3-D image reconstruction of cores and spikeless cores. Final reconstructions of spikeless cores (A, B) and cores (C, D) of reovirus T3D were generated at 28-Å resolution. A difference map representing densities found in cores but not spikeless cores (E, F) was generated at the same resolution. Surface-shaded representations viewed down one icosahedral twofold axis (A, C, E) and twofold cross-sectional representations (B, D, F) are shown for each. Axes of symmetry are marked on the difference map cross section (F) and can be directly translated to the other cross sections. Arrowheads indicate a ring of dsRNA density visible in each cross-sectional view. Arrows indicate the transcriptase-associated density visible in each cross-sectional view. Bar, 20 nm.

differences around the 12 fivefold axes, where the outwardly protruding $\lambda2$ spikes in cores (Figs. 3C and 3D) were missing from the sequentially treated particles (Figs. 3A and 3B). This dramatic difference is the basis for naming these particles "spikeless cores" (a term introduced by Hazelton and Coombs (1999) to describe a $\lambda2$-deficient core-like particle that accumulates at nonpermissive temperatures in cells infected with reovirus mutant tsA279). In contrast, no major differences were noted in the arrangement or relative density of either the underlying $\lambda1$ protein shell or the 150 surface nodules of $\sigma2$ protein, which bind atop $\lambda1$ at positions distinct from those occupied by $\lambda2$ in cores. In cross-sectional views of the core and spikeless-core reconstructions (Figs. 3B

and 3D), interior features attributable to the genomic dsRNA (arrowheads) and transcriptase complexes (arrows) also appeared very similar in the two particles, consistent with the presence of unaltered levels of these components by gel and immunoblot. Moreover, the similarities in all features below a particle radius of 290 Å were evident in radially averaged electron-density plots of the two reconstructions (Fig. 4). Particularly notable were the series of small peaks ascribed to the concentric rings of genomic dsRNA at radii below 250 Å, which were present in the same numbers (eight), and with almost identical intensities and spacings, in the two particles (Fig. 4). Differences above a radius of 290 Å in the radial density plots of the two particles are attributable to the presence or absence of $\lambda2$.

To assist in identifying other changes in the structure of spikeless cores, a difference map between the core and the spikeless core reconstructions was generated (Figs. 3E and 3F). The only significant features in the difference map were 12 structures representing the 12 pentameric spikes of $\lambda2$ that had been removed from cores during the sequential treatments. The absence of other significant features in the difference map suggested again that there are limited changes in the $\lambda1$ shell and $\sigma2$ surface nodules in spikeless cores compared with untreated cores. We placed the crystal-derived structure of the core-bound $\lambda2$ pentamer (Reinisch et al., 2000) into one of the 12 difference-map features (see Materials and Methods). All regions of $\lambda2$ were found to coincide closely in this analysis (Fig. 5). The coincident features included those at the base of the $\lambda2$ spike, near its sites of interaction with $\lambda1$ and $\sigma2$. Thus, we found no evidence that changes in the $\lambda1$ shell or $\sigma2$ nodules contribute features to the difference map.
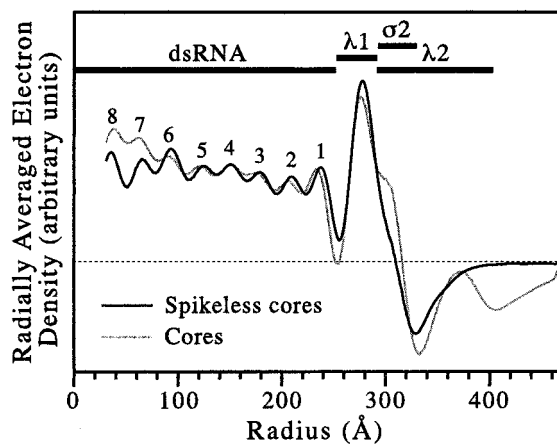

FIG. 4. Radially averaged electron-density plots of the core and spikeless-core reconstructions. Values below a radius of 30 Å were excluded as artifactual. The dotted line indicates an averaged radial density value of zero. The approximate ranges of radii at which dsRNA, $\lambda1$, $\sigma2$, and $\lambda2$ are found in the particles are indicated by horizontal lines above the plots. The rippling peaks attributable to eight concentric rings of genomic dsRNA in each reconstruction are numbered.
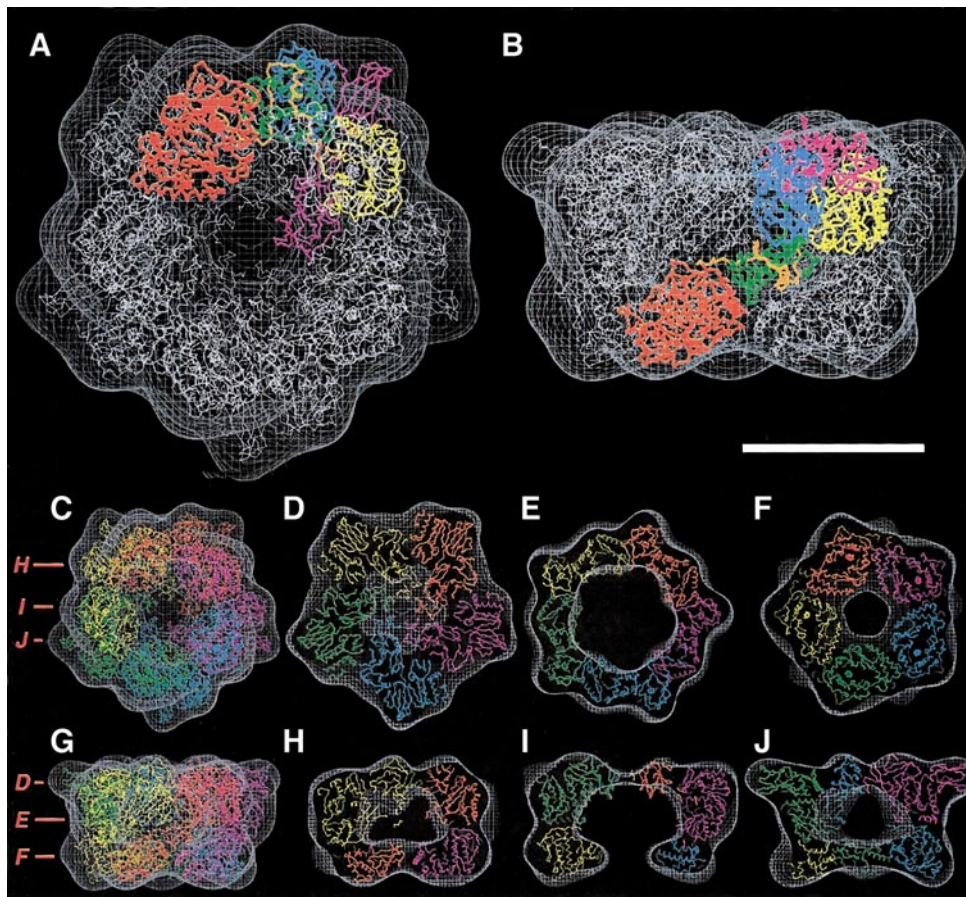
FIG. 5. Comparing the crystal structure of λ2 with the cryo-TEM difference map. The difference map is shown as a hatched net. The crystal structure of the λ2 pentamer is displayed in backbone format. (A, B) Four of the λ2 subunits are shown in white, whereas one subunit is color-coded by domain or region, listed from N- to C-terminus relative to the λ2 primary sequence: red, GTase domain (residues 1–380); orange, extended region (residues 381–433); yellow, N-terminal methyltransferase domain (residues 434–691), green, domain of unknown function (residues 692–805); cyan, more C-terminal methyltransferase domain (residues 806–1022), and magenta, flap domains (residues 1023–1289). The view in A is from the bottom of the λ2 spike relative to the core shell. The fitted structures as viewed in A were rotated toward the viewer by 90° to generate the side view in B. (C–J) Each of the five λ2 subunits is shown in a different color: red, yellow, green, cyan, or magenta. The bottom and side views of the spike in C and G are equivalent to those in A and B. Slab views of the fitted structures at different radii were also generated as indicated by the hash marks at left and are shown in D to F (viewed from bottom of the spike) and H to J (viewed from side of the spike). Bar, 5 nm for top row and 10 nm for bottom two rows.

In a final effort to detect changes in the λ1 shell that may accompany the loss of λ2, we displayed the core and spikeless-core reconstructions over a range of density contours to reveal regions that may differ in electron density between the two particles. Most parts of λ2 and σ2 were removed from these images by radial cropping to permit unobstructed views of the shell. A pore through the shell at the icosahedral fivefold axis, visible in the core crystal structure (Reinisch et al., 2000), was not seen in either particle (Fig. 6). The absence of this pore may reflect an artifact of the averaging used to obtain the reconstructions, and as a result the relative openness of this pore in the two particles could not be addressed. In contrast, pores through the shell beneath the λ2 GTase domains, which are also evident in the core crystal structure (Reinisch et al., 2000; see Fig. 10), became visible when the contour level was raised by only a small

amount for T3D cores (Fig. 6F), as previously described for type 1 Lang (T1L) cores (Spencer et al., 1997). These pores were not visible in the T3D spikeless cores displayed at even higher contour levels (Figs. 6B–6D), suggesting a conformational change in λ1. These results provide evidence that changes in the λ1 shell do indeed accompany the loss of λ2. The basis and significance of these changes, including the elimination of pores through the shell, are addressed in the Discussion.

Scanning cryo-electron microscopy shows rare residual spike structures in spikeless cores

Since the 3-D reconstruction of spikeless cores represents an average of data from multiple particles (Baker et al., 1999), structural features unique to individual particles were lost. As a result, the structure of the residual
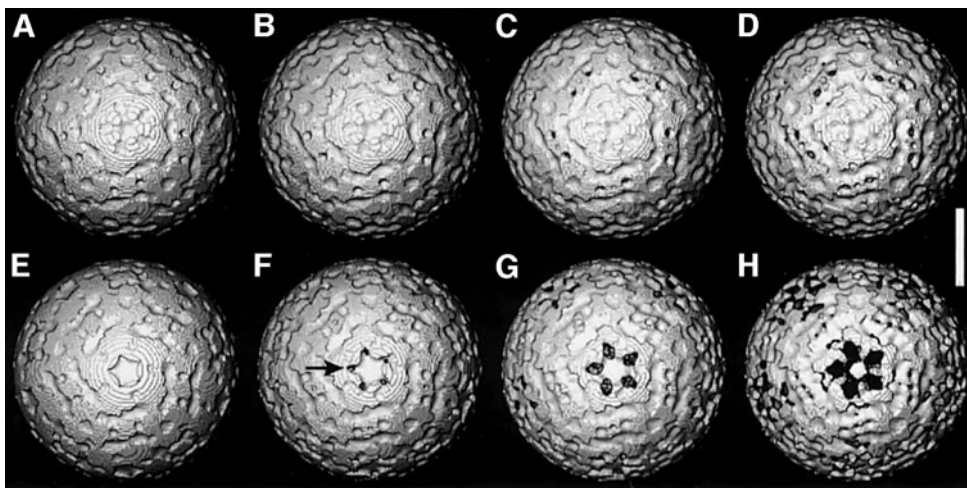
FIG. 6. 3-D reconstructions of cores and spikeless cores displayed at different density contours. Density-scaled reconstructions of T3D spikeless cores (A–D) and cores (E–H) were radially cropped at 29 Å from the particle center and displayed as surface views down a fivefold axis. Different density contour levels, indicated by arbitrary units of −60 (A, E), −70 (B, F), −80 (C, G), and −90 (D, H), were applied to each particle. One of the pores surrounding the fivefold axis in T3D cores, but not spikeless cores, is indicated with an arrow. Bar, 20 nm.

low levels of full-length λ2 in spikeless cores could not be addressed by that approach. Therefore, scanning cryo-electron microscopy (cryo-SEM) was performed to visualize the surface features of individual spikeless cores (Centonze *et al.,* 1995). The majority (94%) of spikeless cores lacked any detectable λ2 spike structures. Of the remaining particles, 2% contained one and 4% contained two evident spikes (Fig. 7). Because only 5 or 6 of the 12 icosahedral fivefold axes can be visualized in any
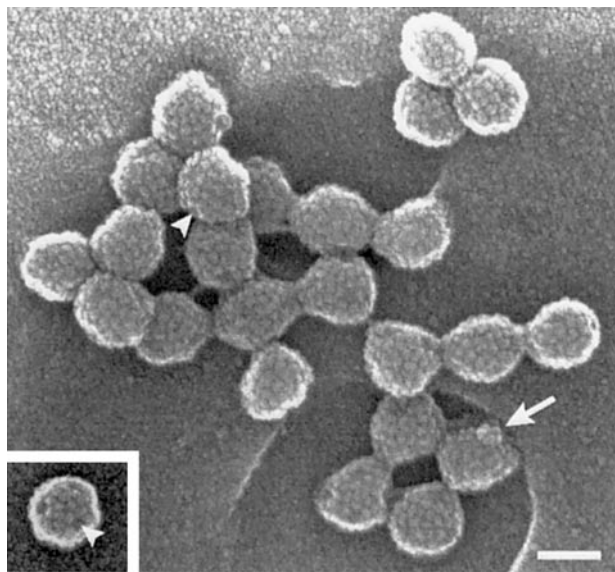

FIG. 7. Cryo-SEM of purified spikeless cores. The fivefold axes of symmetry on the majority of particles are dimpled in appearance (arrowheads) due to the lack of the λ2 spike structure. A residual λ2 spike is visible on a single particle (arrow). The particles appear to interact with one another at the fivefold axes of symmetry, the position of the λ2 pentamer in cores. Individual spikeless cores were observed at low frequency (inset). Magnification, 150,000×. Bar, 50 nm.

single particle by cryo-SEM, λ2 spike structures were calculated to have been detected at only 1.6 to 1.9% of the observed fivefold axes. This frequency of spikes is similar to the amount of full-length λ2 protein in spikeless cores as determined in the autoguanylylation assay (3.6%). Hence, this result suggests that much of the residual λ2 protein remained particle-associated in the form of intact, pentameric spike structures. This result indicates that the residual spikes are stable oligomeric structures because all five of their λ2 subunits remained refractory to disruption during the treatments used to generate spikeless cores. The mechanism by which this subset of λ2 spikes resisted disruption remains unknown.

Another feature of spikeless cores observed by cryo-SEM was the formation of clumps of particles (Fig. 7). These clumps ranged in size from 4 to greater than 50 particles (data not shown). Individual spikeless cores were rarely observed. In contrast, unaggregated core particles are more commonly observed with this technique, and small clumps of cores occur infrequently and range in size from only 2 to 10 particles (Centonze *et al.,* 1995). This difference in particle behavior suggests that removal of λ2 unmasks regions of λ1 or σ2 that promote interparticle associations. Consistent with this idea, core-like particles generated from recombinant λ1 and σ2 proteins in the absence of λ2 show a greater tendency to aggregate than those containing λ2 (J. Kim and M. L. Nibert, unpublished data).

Spikeless cores lack RNA nucleoside-*7N*-methyltransferase activity

The pentameric form of λ2 in reovirus cores is implicated in mediating both the RNA nucleoside-7*N*- and the
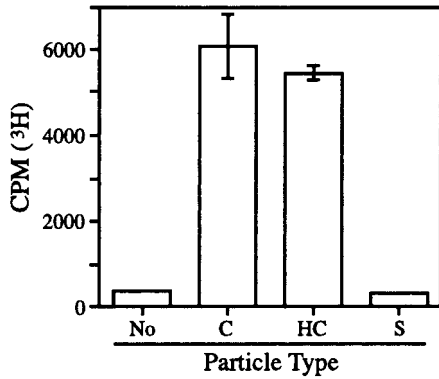
FIG. 8. Quantitative analysis of RNA cap methylation by spikeless cores. Cores (C), HC-cores (HC), and spikeless cores (S) were analyzed. Cap methylation was analyzed by the incorporation of [³H]methyl from [³H-*methyl*]SAM into transcripts. Transcripts were precipitated with TCA and the extent of ³H incorporation was quantitated by scintillation counting. A no-particle control reaction containing storage buffer alone was also analyzed (No). Reactions were performed in triplicate to give the means and standard deviations (error bars) shown on the graph.

RNA nucleoside-2′*O*-methyltransferase activities required for cap 1 formation on reovirus transcripts (Reinisch *et al.,* 2000). The availability of spikeless core particles provided a means to test the role of λ2 in these activities. The capacity of cores to transfer the methyl group from SAM to externally supplied GpppRNA (Furuichi *et al.,* 1977; Mao and Joklik, 1991; Morgan and Kingsbury, 1981) was extended to assay for RNA methyltransferase activity by spikeless cores. Reovirus GpppRNA and [³H-methyl]SAM were incubated with cores, HC-cores, spikeless cores, and a control sample containing no particles. The amount of ³H incorporated into acid-precipitable RNA was quantitated by scintillation counting. In contrast to cores and HC-cores, spikeless cores lacked detectable activity in this assay (Fig. 8). This lack of activity by spikeless cores is consistent with a requirement for λ2 in at least the nucleoside-7*N*-methyltransferase function in RNA capping. Since the product of the nucleoside-7*N*-methyltransferase reaction, ᵐGpppRNA (cap 0), is the substrate for the nucleoside-2′*O*-methyltransferase (Furuichi *et al.,* 1976), the role of λ2 in the latter activity could not be addressed in these experiments.

λ2 spike loss correlates with loss of transcription and other core activities

Having demonstrated loss of λ2 from spikeless cores, but retention of high levels of the other core components and integrity of other aspects of particle morphology, we investigated whether the reovirus transcription enzymes remained functional in spikeless cores. Measurement of [α-³²P]CTP incorporation into acid-precipitable RNA demonstrated that transcription activity in spikeless cores was less than 2% of that in cores or HC-cores (Fig.
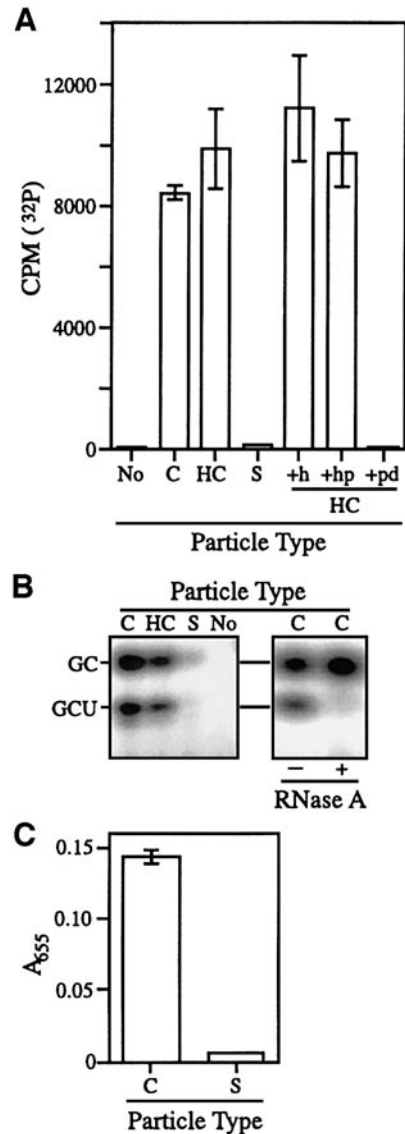

FIG. 9. Analysis of transcription, abortive oligonucleotide synthesis, and ATPase activities in spikeless cores. The following particles were analyzed in particular experiments: cores (C), HC-cores (HC), spikeless cores (S), HC-cores additionally treated with heat alone (+h), HC-cores additionally treated with heat and the protease CHT (+hp), and HC-cores additionally treated with the protease CHT and the detergent STS (+pd). A no-particle control reaction containing storage buffer alone was also analyzed (No). (A) Transcription. Transcription activity was quantitated by liquid scintillation counting from the amount of ³²P incorporated from [α-³²P]CTP into TCA-precipitable material. Reactions were performed in triplicate to give the means and standard deviations (error bars) shown on the graph. (B) Abortive oligonucleotide synthesis. Abortive transcription activity was demonstrated by phosphorimager analysis from the amount of ³²P incorporated from [α-³²P]CTP into oligonucleotide bands resolved by gel electrophoresis. The GCU oligonucleotide is distinguished by its susceptibility to cleavage by RNase A at right. (C) ATP hydrolysis. ATPase activity was quantitated by colorimetric assay for free phosphate ion. Samples containing ATP alone were included to permit correction for background attributable to phosphate release by nonenzymatic hydrolysis of ATP. Reactions were performed in triplicate to give the means and standard deviations (error bars) shown on the graph.

9A). Though spikeless cores showed a greatly reduced capacity to produce elongated, acid-precipitable RNAs, they might still be capable of initiating transcription and producing shorter transcripts. Reovirus cores are known to generate two- to four-nucleotide abortive transcripts at a rate 5- to 100-fold higher than full-length transcripts (Yamakawa *et al.,* 1981). Detection of these products provides a sensitive assay for transcription initiation. We therefore assayed for incorporation of $[\alpha\text{-}^{32}P]CTP$ into GC and GCU, the primary abortive transcripts (Farsetta *et al.,* 2000; Yamakawa *et al.,* 1981), and found that spikeless cores retained only 6.6% ($\pm$2.5%) of the level of transcription initiation by cores (Fig. 9B). Thus, spikeless cores obtained with our sequential treatment protocol exhibit severely reduced transcription initiation activity, consistent with the low transcription activity of spikeless cores obtained by high pH treatment (White and Zweerink, 1976).

Reovirus cores show NTPase activity indicative of the putative RNA helicase or RNA 5′ triphosphatase roles of the $\lambda 1$ protein (Bisaillon *et al.,* 1997; Bisaillon and Lemay, 1997; Noble and Nibert, 1997a). The $\mu 2$ protein also contributes to the NTPase activity of cores (Noble and Nibert, 1997b). Since $\lambda 1$ and $\mu 2$ are present at similar levels in spikeless cores and cores, our expectation was that both particles would mediate similar levels of ATPase activity. The activity was analyzed using a sensitive colorimetric assay, which measures the amount of phosphate released upon ATP hydrolysis (Noble and Nibert, 1997a). ATPase activities in cores and spikeless cores were measured at pH 8.5 and 35°C as well as at pH 6.5 and 55°C to discriminate the contributions of $\lambda 1$ and $\mu 2$ (Noble and Nibert, 1997b). At pH 8.5 and 35°C, spikeless cores exhibited less than 4% of the ATPase activity of cores (Fig. 9C). At pH 6.5 and 55°C their ATPase activity was less than 2% that of cores (data not shown). Thus, the absence of $\lambda 2$ in our spikeless cores also correlates with a severe reduction in ATPase activity.

Relative roles of heat, protease, and detergent in loss of transcription activity from spikeless cores

Because HC-cores retain full transcription activity (Luongo *et al.,* 1997) (Fig. 9A), it was unlikely that the second exposure to heat or the second exposure to CHT by itself caused spikeless cores to lose transcription activity. To identify the specific effects of each of these treatments, we subjected HC-cores to heat alone or to heat followed by CHT digestion. Particles were recovered by centrifugation in a CsCl gradient and assayed for transcription activity. Both particle types retained full transcription activity (Fig. 9A). Both particle types also retained large amounts of the 120K N-terminal fragment of $\lambda 2$ (data not shown). However, incubation of HC-cores with CHT and STS without prior heat treatment led to recovery of par-

ticles after equilibrium centrifugation in which transcription activity was greatly reduced (Fig. 9A). These particles lacked the 120K $\lambda 2$ fragment (data not shown) and thus demonstrated that the second round of heat treatment is not necessary for removing this fragment. The effect of STS treatment alone was explored by heating HC-cores and then exposing them to 0.5 mM detergent. These particles did not form bands after centrifugation in a CsCl gradient, rendering further analysis impossible. Particles were alternatively treated with 0.5 mM STS (above the critical micellar concentration for this detergent) and then diluted to 0.1 mM STS (below its critical micellar concentration) (Chandran and Nibert, 1998) by addition to a transcription reaction. Cores or HC-cores treated in this manner retained only 3 or 0.4%, respectively, of the transcription activity of the respective particles exposed to only 0.1 mM STS (data not shown). For both particles, the $\lambda 2$ protein and/or 120K N-terminal fragment remained particle-bound after centrifugation through sucrose (data not shown), indicating that $\lambda 2$ loss is not strictly required for loss of transcription activity. However, since exposure to micellar concentrations of STS is known to alter $\lambda 2$ conformation, as indicated by the degradation of $\lambda 2$ once CHT is added, conformational change in $\lambda 2$ remains correlated with the loss of transcription.

Binding recombinant $\lambda 2$ protein to spikeless cores

A hypothesized use for spikeless cores was the development of a molecular-genetic approach for analyzing $\lambda 2$ functions in core-like particles, similar to strategies developed for outer-capsid proteins $\mu 1$, $\sigma 3$, and $\sigma 1$ in virion-like particles (Chandran *et al.,* 1999, 2001; Jané-Valbuena *et al.,* 1999). In such "recoating" experiments we envisioned removing $\lambda 2$ from cores to generate spikeless cores that retain the viral genome but lack activities in transcription and capping. Subsequent binding of recombinant $\lambda 2$ to these particles *in vitro* might be expected to allow recovery of one or more of the missing activities. The use of specific mutant forms of recombinant $\lambda 2$ could then be used to identify important $\lambda 2$ sequence determinants for these activities. The use of spikeless cores as a substrate for $\lambda 2$ binding was tested by incubating such particles with lysate from insect cells infected with a recombinant baculovirus that expressed wild-type $\lambda 2$ protein (Luongo *et al.,* 1998). Though analyses of the particles purified from such reactions showed greater binding of recombinant $\lambda 2$ protein to spikeless cores than to cores, the bound $\lambda 2$ exhibited negligible autoguanylylation activity and did not form spike-like structures visible by cryo-SEM (data not shown). Also, these putatively recoated particles showed negligible transcription activity (data not shown). Hence, recombinant $\lambda 2$ protein appears to bind to spikeless cores in a manner that does not permit recovery of the

missing core activities, and this type of particle preparation is apparently not suitable for the anticipated molecular-genetic studies of λ2.

DISCUSSION

Reovirus core structure

The structure of our spikeless T3D cores determined by cryo-electron microscopy is consistent with the core structure determined by X-ray crystallography (Reinisch et al., 2000). The core crystal structure indicates that the λ2 pentamers bind to the outer surface of the λ1 shell, suggesting that the λ2 spikes might be detached from this shell without destroying the basic integrity of the particle. The current study confirms that λ2 is not required for the integrity of the core shell in previously assembled particles, in that removal of λ2 did not affect the basic appearance of the shell at 28-Å resolution or the gel-defined abundance of the other particle components including the genomic dsRNA. Other findings indicate that λ2 is not required for assembly of the core shell containing λ1 and σ2 (Xu et al., 1993; J. Kim and M. L. Nibert, manuscript in preparation).

The findings in this study corroborate a view of the organization of proteins in reovirus cores indicated by the crystal structure (Reinisch et al., 2000). In particular, the recent data show that the core shell per se is formed by λ1 alone, with λ2 and σ2 binding to its outer surface and making no direct contributions to the T = 1 lattice. Thus, the σ2 nodules and the similarly nodule-like N-terminal GTase domain of λ2 (Reinisch et al., 2000) (seen tangential to the shell in cross sections (Figs. 3D and 3F)) can be considered to form an incomplete middle layer of protein in reovirus virions, between the T = 1 inner layer formed by λ1 and the T = 13 outer layer formed by μ1 (Dryden et al., 1993). The more C-terminal regions of λ2 project into the outer layer and make direct contributions to the T = 13 lattice at its peripentonal positions (Dryden et al., 1993) such that λ2 can be considered an outer-capsid component as well. Unlike λ2, σ2 appears to be required for assembly of a stable core shell (Xu et al., 1993; J. Kim and M. L. Nibert, manuscript in preparation). Whether σ2 can be removed from the previously assembled shell without destroying its basic integrity, as can λ2, remains to be determined.

The cross-sectional views of the 3-D reconstructions of both cores and spikeless cores show density in concentric rings within the central region occupied by the genomic dsRNA (Figs. 3B, 3D, and 4). In each particle type, eight rings of putative RNA density are distinguishable, indicative of similar separations between rings within the two particles and consistent with the fact that spikeless cores appear by gel to have retained approximately core-like levels of the 10 dsRNA segments (Fig. 2C). The average center-to-center distance between adjacent rings in each reconstruction is 26–28 Å. This finding is reminiscent of results from low-angle X-ray diffraction studies of reovirus particles (Harvey et al., 1981), close-to focus cryo-electron micrographs of reovirus cores (Dryden et al., 1993), and the reovirus core crystal structure (Reinisch et al., 2000), all showing densities separated by 25–27 Å within the RNA region and indicative of RNA packing with statistical order to fill the available space (Reinisch et al., 2000). The cross-sectional views of both cores and spikeless cores also show evidence of the transcriptase complexes anchored to the λ1 shell at or near each fivefold axis (Dryden et al., 1998).

Potential role of λ2 in reovirus transcriptase activity and its structural basis

As expected for particles lacking the enzymatically active λ2 protein (Cleveland et al., 1986; Luongo et al., 1998, 2000; Mao and Joklik, 1991; Reinisch et al., 2000; Shatkin et al., 1983), spikeless cores were shown in this study to lack the RNA GTase (Figs. 1 and 2A) and RNA nucleoside-7N-methyltransferase (Fig. 8) activities that are required for formation of a cap 1 structure on viral transcripts. The effects of λ2 removal on transcription and ATP hydrolysis by spikeless cores are not as easily explained, however, because these activities are ascribed to core proteins λ1, λ3, and μ2 (Bisaillon et al., 1997; Bisaillon and Lemay, 1997; Morozov, 1989; Noble and Nibert, 1997a, b; Starnes and Joklik, 1993; Yin et al., 1996), which are found at normal levels in spikeless cores (Fig. 2B). Heat and CHT treatment, which removes only a 24K C-terminal portion of λ2 (Luongo et al., 1997), has no effect on transcription (Luongo et al., 1997) (Fig. 9A) or ATP hydrolysis (T. J. Broering and M. L. Nibert, unpublished data). These observations suggest that effects on more N-terminal regions of λ2 are required for loss of transcription activity.

Contacts of λ2 with λ1 and σ2 in cores are made exclusively through the 42-kDa N-terminal GTase domain of λ2 at the base of the λ2 spike (Luongo et al., 2000; Reinisch et al., 2000; Breun et al., 2001) (Fig. 5; also see Fig. 10). Loss of transcription and ATPase activities observed in the present study may thus be specifically attributable to changes in other core proteins resulting from loss or alteration of their interactions with this specific λ2 region. Though the λ3 and μ2 core proteins were not resolved in the core crystal structure (Reinisch et al., 2000), it seems unlikely that either makes direct contacts with λ2 in cores because they are thought to constitute the bulk of the putative transcriptase complexes that are bound beneath the λ1 shell near the icosahedral fivefold axes (Dryden et al., 1998). Thus, λ3 and μ2 are likely separated from λ2 by the thickness of the λ1 shell (Reinisch et al., 2000). Loss of transcription and ATPase activities in spikeless cores may nonetheless be explained by local alterations in the λ1 shell that result when the interactions of λ2 with λ1 and/or σ2 are
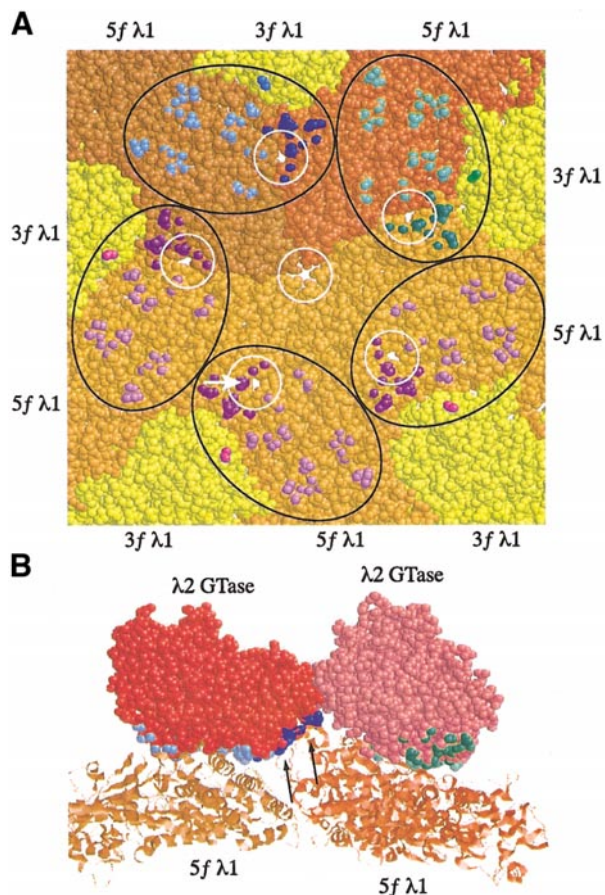
FIG. 10. λ1–λ2 interactions in the core crystal structure. The crystal structure of the reovirus core (Reinisch *et al.,* 2000) is shown at the same scale in both panels. (A) The fivefold-proximal portions of one λ1 decamer unit are shown in space-filling format. The five fivefold-proximal subunits of λ1 are colored brown-orange, red-orange, and orange and are labeled on the periphery. The five interdigitating threefold-proximal subunits of λ1 are colored yellow and are labeled on the periphery. The pores at and surrounding the fivefold axis are enclosed by white circles. A white arrow points to the same pore as the arrow in Fig. 6F. The approximate footprints of the five overlying λ2 GTase domains are shown as black ovals. Atoms in λ1 that approach within 4.0 Å of atoms in the λ2 GTase domains are highlighted with different colors. For each λ2 GTase domain, the approaching atoms in λ1 are highlighted with a light color (light blue, light green, or light purple) on the fivefold-proximal λ1 subunit on which the GTase domain primarily sits, with a dark shade of that color (dark blue, dark green, or dark purple) on the adjacent fivefold-proximal λ1 subunit that the GTase domain contacts and with an intermediate shade of that color on the interdigitating threefold-proximal λ1 subunit that the GTase domain touches. (B) The brown-orange and red-orange fivefold-proximal λ1 subunits from A are shown in ribbon format along with their overlying λ2 GTase domains in space-filling format. The bottom of the view in A was rotated 80° toward the reader to generate this view. Atoms in λ2 that approach within 4.0 Å of atoms in λ1 are highlighted with different colors that match those used for the λ1 atoms they approach as highlighted in A (i.e., light to light and dark to dark). Projecting regions of the λ1 subunit (red-orange) that contact the adjacent λ2 GTase domain (pink) are indicated by black arrows.

altered or lost and that may cause further changes in the underlying transcriptase complexes. For example, given the reduction in all transcription-related activities by spikeless cores, including abortive transcript production, disengagement of the dsRNA genome segments from the RNA polymerase protein λ3 in spikeless cores is a possibility worth investigating in future studies. According to this proposed explanation, λ2 may play an important role in reovirus transcription by stabilizing the transcriptase complexes in a functional conformation through protein–protein and/or protein–RNA interactions within the core.

The analysis of cores and spikeless cores at different density contours identified some changes in the λ1 shell associated with λ2 loss (Fig. 6), consistent with one or more of the preceding possibilities to explain the loss of transcriptase and NTPase activities by spikeless cores. The finding that pores through the λ1 shell beneath the λ2 GTase domains are less open in spikeless cores suggests that plugging of these pores may explain at least some of those particles' lost functions. The pores in question are evident in the core crystal structure (Reinisch *et al.,* 2000). Each GTase domain in the λ2 pentamer mediates major contacts with two adjacent fivefold-proximal subunits of λ1 (Figs. 10A and 10B) and a minor contact with the interdigitating threefold-proximal subunits of λ1 (Fig. 10A) in the λ1 decamer unit (Reinisch *et al.,* 2000). The footprint of each λ2 GTase domain (Fig. 10A, black ovals) overlies the intersection of these three copies of λ1. Thirty-one different λ1 residues (Fig. 10A) are likely involved in these contacts, as judged by their approach to within 4.0 Å of 32 different residues in each respective λ2 GTase domain (Breun *et al.,* 2001) (Fig. 10B). By having removed λ2 from these contacts in spikeless cores, small shifts in the positions of the λ1 subunits may occur and result in further changes inside the shell. The contacts of each λ2 GTase domain with the fivefold-proximal λ1 subunit adjacent to the one on which it primarily sits (Figs. 10A and 10B) are mediated through two projecting regions of λ1 structure: a loop (residues 661–667) and a bent α-helix (residues 686–698) (Fig. 10B, arrows). Upon removal of λ2 from these contacts, these projecting regions of λ1 may collapse. Interestingly, these regions of λ1 in cores project beside a pore (Fig. 10A, peripheral white circles) that opens into the core interior and corresponds to the pores observed in cores, but not spikeless cores, in cryo-TEM reconstructions (Fig. 6). Collapse of these regions of λ1 may therefore plug the top of this pore. The relative roles of this pore and the one at each fivefold axis (Fig. 10A, central white circle) in substrate (nucleoside triphosphate; NTP) entry and product (plus-strand RNA) and by-product (pyrophosphate, phosphate, and NDP) release during reovirus mRNA synthesis remain to be addressed (Reinisch *et al.,* 2000; Spencer *et al.,* 1997), but these pores may be key targets for regulation of core functions. One possible explanation is that the pores that open beneath each λ2 GTase domain in cores may be essential for NTP entry to the core interior and, by being plugged upon λ2 release

from spikeless cores, may cause all NTP-dependent activities to cease.

Recent data indicate that addition of reovirus outer-capsid proteins μ1 and σ3 to cores to produce recoated, virion-like particles blocks the transition from initiation to elongation during transcription (Farsetta *et al.,* 2000). That study therefore provides other evidence that reovirus transcription activity can be affected across the intervening λ1 shell, possibly as translated through either λ2 or σ2, which are both believed to contact the μ1 outer-capsid protein in virion-like particles (Dryden *et al.,* 1993; Reinisch *et al.,* 2000). This regulation of core activities by μ1 and σ3 could conceivably also involve the opening and closing of specific pores through the λ1 shell.

The 3-D reconstruction of reovirus T3D cores in this study is notable in that no pore is evident through the topmost "flaps" of the λ2 spike (Fig. 3D). This was also noted for T3D cores in a previous cryo-TEM reconstruction (Luongo *et al.,* 1998) and contrasts with the more open conformation of the spike first noted with T1L cores (Dryden *et al.,* 1993). The crystal structure of reovirus cores shows the outer portion of λ2 in the closed conformation, which may be characteristic of the T3D λ2 protein in cores since the crystal structure was determined for cores of T1L $\times$ T3D reassortant virus F18, which contain T3D-derived λ2 (Reinisch *et al.,* 2000). The basis for the conformational variability of this outer region of λ2 structure and its significance for the release of nascent capped transcripts through the top of the λ2 spike (Bartlett *et al.,* 1974; Yeager *et al.,* 1996) remain important questions.

Assembly of λ2 and molecular-genetic studies of λ2 functions in particles

Our failure to reconstitute enzymatically active particles by recoating spikeless cores with recombinant λ2 is disappointing, but might be explained and perhaps corrected in several different ways. One possibility is that the binding sites for λ2 in spikeless cores were disrupted by detergent during preparation of these particles. In that case, a new protocol to generate genome-containing spikeless cores in the absence of detergent may yet allow the recoating approach to succeed. Another possibility is that λ2 requires another cellular or viral factor, absent from the recoating protocol, for binding to the core shell. For example, Hazelton and Coombs (1999) proposed that preformed complexes of λ2 pentamers and σ1 trimers are the likely substrates for assembly onto the core shell within infected cells. Recombinant λ2 protein, including that used in this study, is known not to form pentamers on its own (Luongo *et al.,* 2000; Mao and Joklik, 1991). Accordingly, we might find that addition of recombinant σ1 protein to the recoating procedure might yet allow this approach to work. The generation of core-like particles from coexpressed λ1, λ2, and σ2 core proteins (Xu *et al.,* 1993; J. Kim and M. L. Nibert, manuscript in preparation), however, suggests that a specific requirement for σ1 in λ2 assembly into cores is unlikely.

Other interpretations of our failure to recoat spikeless cores with recombinant λ2 suggest less optimism for future success. For example, the effects of λ2 removal on the λ1 shell (Figs. 6 and 10) may not only explain the reductions in spikeless core transcription and NTPase activities but may also render the λ1 protein incompetent for subsequent rebinding of λ2. It may therefore be that λ2 can be assembled into cores only as the shell is being formed, i.e., before maturation of the final $T = 1$ structure. Other approaches, such as the generation of core- or virion-like particles wholly from recombinant proteins (Xu *et al.,* 1993; J. Kim and M. L. Nibert, manuscript in preparation), may therefore prove more useful for molecular-genetic studies of at least some λ2 functions, including those in RNA capping.

MATERIALS AND METHODS

Reagents

All enzymes and chemicals were from Sigma Chemical Co. unless otherwise stated. The electrophoresis and immunoblot reagents and rigs were from Bio-Rad Laboratories. Nucleotides were obtained from Pharmacia Biotech. All radiolabeled reagents were from Dupont NEN.

Generation of cores, HC-cores, and spikeless cores

Virions of reovirus T3D were purified as described (Furlong *et al.,* 1988), and their concentrations were determined from the relationship 1.0 A_{260} = 2.1 $\times$ 10^{12} virions/ml (Smith *et al.,* 1969). Cores of reovirus were prepared by digesting virions at a concentration of 3 $\times$ 10^{13} particles/ml with 200 μg/ml α-CHT for 1.5 h at 37°C in storage buffer (10 mM Tris, pH 7.5, 10 mM MgCl$_2$, 150 mM NaCl) (Luongo *et al.,* 1998). The CHT was inactivated by addition of 1 mM phenylmethylsulfonyl fluoride (PMSF). To purify cores, digests were loaded onto preformed CsCl gradients (ρ = 1.30 to 1.55 g/cm^3) and subjected to equilibrium centrifugation. The particles were dialyzed into storage buffer and stored at 4°C. Core concentrations were determined from the relationship 1.0 A_{260} = 4.4 $\times$ 10^{12} cores/ml (Coombs, 1998).

HC-cores were generated as described (Luongo *et al.,* 1997). In brief, 1 $\times$ 10^{13} cores in storage buffer were heated to 52°C for 30 min, cooled to 37°C, and treated with 200 μg/ml CHT for 10 min. Following treatment, the CHT was inactivated with 1 mM PMSF, and the HC-cores were isolated following equilibrium centrifugation as described for cores. The particles were dialyzed into storage buffer and stored at 4°C.

Spikeless cores were generated by heating 1 $\times$ 10^{13} or

2×10^{13} cores or HC-cores, respectively, in storage buffer to 52°C for 30 min, cooling to 37°C, and treating with 200 μg/ml CHT and 0.5 mM STS for 10 min. Following treatment, the CHT was inactivated with 1 mM PMSF. To purify the particles, digests were loaded onto a CsCl gradient (ρ = 1.30 to 1.55 g/cm³) that had been overlaid with 20% (w/v) sucrose equaling one-third of the final gradient volume. After centrifugation at 55,000 rpm in a Beckman SW60Ti rotor at 5°C for greater than 2 h, the particles were recovered as an optically homogeneous band. The particles were dialyzed into storage buffer and stored at 4°C.

SDS–PAGE

Samples were prepared for SDS–PAGE by mixing in a 2:1 (v/v) ratio with 3× Laemmli sample buffer (3% SDS, 9% β-mercaptoethanol, 375 mM Tris, pH 8.0, 30% sucrose, and 0.004% bromophenol blue). Samples were incubated at 60°C for 3 min (for protein and dsRNA analysis) or boiled for 2 min (for protein analysis). Equal volumes of samples were then subjected to electrophoresis in an 8% polyacrylamide Tris–glycine–SDS gel. Proteins were stained with Coomassie brilliant blue R-250. After Coomassie staining in some cases, the dsRNA was stained with 2% methylene blue in 0.1× TAE buffer.

Autoguanylylation analysis

Reaction mixtures (10 μl) containing 1×10^{11} particles (added to the reaction mixture in 2 μl storage buffer), 50 mM Tris–HCl, pH 8.0, 10 mM MgCl$_2$, 2 mM dithiothreitol (DTT), and 5 μCi of [α-^{32}P]GTP (3000 Ci/mmol) were incubated for 30 min at room temperature. Reactions were terminated by the addition of 5 μl of 3× Laemmli sample buffer. The reactions were then subjected to SDS–PAGE. Radiolabeled protein was detected in the dried gel by phosphorimager analysis (Molecular Dynamics).

Immunoblot analyses

Equivalent amounts of particles in triplicate were subjected to SDS–PAGE. Proteins in the gel were transferred to nitrocellulose by electroblotting at 100 V for 1.5 h at 4°C with 25 mM Tris, 192 mM glycine, pH 8.3, buffer in a minigel transfer apparatus. The membrane was divided into three equivalent strips. Individual strips were probed with a 1/1000 dilution of a polyclonal anti-λ3 antiserum (D. L. Farsetta and M. L. Nibert, unpublished data), a polyclonal anti-core antiserum to detect λ1 and σ2 (Chandran et al., 1999), or a polyclonal anti-μ2 antiserum (Zou and Brown, 1996). The polyclonal antibodies were bound by goat anti-rabbit antibodies conjugated with alkaline phosphatase and visualized colorimetrically with Nitro blue tetrazolium and 5-bromo-4-chloro-3-indolyl phosphate.

Cryo-electron microscopy and 3-D image reconstructions

For cryo-TEM, purified particles obtained from reovirus T3D were embedded in vitreous ice, and micrographs were recorded under conditions of minimal irradiation ($\approx$6 and $\approx$20 electrons/Å² for the core and spikeless core samples, respectively) in Philips CM200 and CM300 FEG microscopes at magnifications of ×27,500 and ×45,000. The micrograph of spikeless cores was recorded with minimal astigmatism at 3.1 μm under focus, whereas the micrograph of cores exhibited astigmatism with 2.0- and 3.3-μm defocus along orthogonal directions. The particle orientations in both micrographs were sufficiently random to satisfy sampling requirements for Fourier inversion: all inverse eigenvalues were <0.10 and more than 99% were <0.01. 3-D image reconstruction procedures were carried out as described (Dryden et al., 1998), with a previous 3-D reconstruction of the reovirus T1L core (Dryden et al., 1993) used as the initial reference for model-based refinement of particle origin and orientation parameters (Baker and Cheng, 1996). Several iterative steps of refinement were conducted until no improvement in resolution beyond 28 Å could be obtained with either data set as determined by various criteria, such as phase residuals and correlation coefficients (Baker et al., 1999). Corrections were applied to compensate for the effects of the microscope contrast transfer function, resulting in the minimization of the effects of the astigmatism in the micrograph of cores (Baker et al., 1999). Final reconstructions were generated at 28-Å resolution using 1454 and 1078 particle images of cores and spikeless cores, respectively. For cryo-SEM, sample preparation, image capture, and processing for publication were undertaken as described (Centonze et al., 1995). Figures 3 and 6 were assembled in Photoshop 5.5 (Adobe Systems).

Placement of the λ2 crystal structure into the cryo-TEM difference map (Fig. 5)

A single λ2 pentamer spike was cut out from the whole 3-D difference map and converted to proper format for use in the program O (Kjeldgaard et al., 1993). Using O, the reovirus core crystal structure (Reinisch et al., 2000) was then moved by eye to obtain an optimal fit within the difference map. Enhanced color images were prepared with the program Bobscript 2.4 (Esnouf, 1997) using the fitted structures output from O. The final figure was assembled in Photoshop 5.5 (Adobe Systems).

Displays of λ1–λ2 interactions from the crystal structure (Fig. 10)

The reovirus core crystal structure (Reinisch et al., 2000) was displayed using RasMac 2.7, including identification of the residues in λ1 and λ2 that approach within

4 Å of the opposite subunit. The final figure was assembled in Illustrator 8.0 (Adobe Systems).

RNA cap methylation

Cap methylation was analyzed *in vitro* as described (Morgan and Kingsbury, 1981). Reovirus GpppRNA was generated from 6.7×10^{12} T3D cores/ml in 100 mM Tris, pH 8.0, 12 mM $MgCl_2$, a 2 mM concentration each of ATP, CTP, and UTP, 0.5 mM GTP, 0.5 mM *S*-adenosyl-L-homocysteine, and 0.02 U/μl inorganic pyrophosphatase (Roche Molecular Biochemicals) by incubation at 40°C for 1.5 h (Furuichi *et al.,* 1976). The reovirus cores were then removed by centrifugation. The RNA was purified by addition of 1% SDS (final) before extraction with warm phenol and ethanol precipitation. The RNA was resuspended in deionized water and its concentration determined by spectrophotometry. For the methylation assay, 6 μg of reovirus GpppRNA was added per 10-μl reaction containing 50 mM Tris, pH 8.0, 10 mM magnesium acetate, 1 mM DTT, 1.5% PEG, 20 U RNasin (Promega), and 0.275 μCi [^{3}H]SAM (80 Ci/mmol). After addition of 2.9×10^{11} particles in 4.8 μl of storage buffer, the reaction mixtures were incubated at 40°C for 2 h. Reactions were terminated by the addition of 10 μg bovine serum albumin and 30 μl of 10% trichloroacetic acid (TCA). Precipitated material was washed with 100 μl of 10% TCA and 200 μl of 55% ethanol and resuspended in 50 mM Tris, pH 8.5, 50 mM KCl by incubation at 65°C overnight. ^{3}H-labeled transcripts in the precipitates were detected by liquid scintillation counting.

Transcription assays

Transcription generating elongated transcripts was analyzed *in vitro* as described (Drayna and Fields, 1982). In brief, reaction mixtures (50 μl) contained 70 mM Tris, pH 8.0, 10 mM $MgCl_2$, a 1 mM concentration each of ATP, CTP, and UTP, 3.5 mM GTP, 0.05 U inorganic pyrophosphatase, 10 mM phosphoenol pyruvate, 0.4 U pyruvate kinase, and 2.5 μCi of [α-^{32}P]CTP (3000 Ci/mmol). Following the addition of 1×10^{11} particles in 20 μl of storage buffer, reaction mixtures were incubated at 45°C for 1 h. Reactions were terminated by the addition of 10 μg bovine serum albumin, 20 μg tRNA (Roche Molecular Biochemicals), and 150 μl of 10% TCA. Precipitated material was washed with 100 μl of 10% TCA and 200 μl of 55% ethanol and resuspended in 50 mM Tris, pH 8.5, 50 mM KCl by incubation at 65°C. ^{32}P-labeled transcripts in the precipitates were detected by liquid scintillation counting.

Transcription generating oligonucleotides was analyzed *in vitro* as described (Yamakawa *et al.,* 1981). In brief, reaction mixtures (15 μl) contained 100 mM Tris, pH 8.3, 4 mM $MnCl_2$, a 1 mM concentration each of ATP, CTP, UTP, and GTP, 3.3 mM phosphoenol pyruvate, 0.8 U pyruvate kinase, 6 U RNasin, 2.5 mM DTT, and 2.5 μCi of [α-^{32}P]CTP. Following the addition of 3×10^{11} particles in 3.2 μl storage buffer, reaction mixtures were incubated at 40°C for 1 h. Reactions were then treated with 20 U of calf intestinal alkaline phosphatase (New England Bio-Labs) at 37°C for 1 h to degrade the labeled CTP. The reaction mixtures were resolved by electrophoresis in a discontinuous 20% polyacrylamide Tris–borate–EDTA–urea gel. Labeled products were detected in the gel by phosphorimager analysis.

ATPase assay

ATPase activity of particles was analyzed *in vitro* as described (Noble and Nibert, 1997a). In brief, reaction mixtures (60 μl) contained 50 mM Tris–morpholinosulfonic acid, 7.5 mM NaCl, 5 mM $MgCl_2$, 1 mM ATP, and 3.6×10^{10} particles. Reactions were incubated for 30 min at pH 8.5 and 35°C or at pH 6.5 and 55°C. Reactions were terminated by the addition of 60 μl of 10% TCA. To measure the amount of free phosphate ion in each sample, 100 μl of the stopped reaction was mixed with 100 μl of 3:1:1 of 0.8% ammonium molybdate:6 N sulfuric acid: 10% (w/v) ascorbic acid and incubated at 37°C for 30 min prior to determination of A_{655}. Samples containing ATP alone were included to permit correction for background attributable to phosphate release by nonenzymatic hydrolysis of ATP.

REFERENCES

Baker, T. S., and Cheng, R. H. (1996). A model-based approach for determining orientations of biological macromolecules imaged by cryo-electron microscopy. *J. Struct. Biol.* **116,** 120–130.

Baker, T. S., Olson, N. H., and Fuller, S. D. (1999). Adding the third dimension to virus life cycles: Three-dimensional reconstruction of

icosahedral viruses from cryo-electron micrographs. *Microbiol. Mol. Biol. Rev.* **63,** 862–922.

Bartlett, N. M., Gillies, S. C., Bullivant, S., and Bellamy, A. R. (1974). Electron microscopy study of reovirus reaction cores. *J. Virol.* **14,** 315–326.

Bisaillon, M., Bergeron, J., and Lemay, G. (1997). Characterization of the nucleoside triphosphate phosphohydrolase and helicase activities of the reovirus λ1 protein. *J. Biol. Chem.* **272,** 18298–18303.

Bisaillon, M., and Lemay, G. (1997). Characterization of the reovirus λ1 protein RNA 5′-triphosphatase activity. *J. Biol. Chem.* **272,** 29954–29957.

Breun, L. A., Broering, T. J., McCutcheon, A. M., Harrison, S. J., Luongo, C. L., and Nibert, M. L. (2001). Mammalian reovirus L2 gene and λ2 core spike protein sequences and whole-genome comparisons of reoviruses type 1 Lang, type 2 Jones, and type 3 Dearing. *Virology* **287,** 333–348.

Centonze, V. E., Chen, Y., Severson, T. F., Borisy, G. G., and Nibert, M. L. (1995). Visualization of individual reovirus particles by low-temperature, high-resolution scanning microscopy. *J. Struct. Biol.* **115,** 215–225.

Chandran, K., and Nibert, M. L. (1998). Protease cleavage of reovirus capsid protein μ1/μ1C is blocked by alkyl sulfate detergents, yielding a new type of infectious subvirion particle. *J. Virol.* **72,** 467–475.

Chandran, K., Walker, S. B., Chen, Y., Contreras, C. M., Schiff, L. A., Baker, T. S., and Nibert, M. L. (1999). In vitro recoating of reovirus cores with baculovirus-expressed outer-capsid proteins μ1 and σ3. *J. Virol.* **73,** 3941–3950.

Chandran, K., Zhang, X., Olson, N. O., Walker, S. B., Chappell, J. D., Dermody, T. S., Baker, T. S., and Nibert, M. L. (2001). Complete in vitro assembly of the reovirus outer capsid produces highly infectious particles suitable for genetic studies of the receptor-binding protein. *J. Virol.* **75,** 5335–5342.

Cleveland, D. R., Zarbl, H., and Millward, S. (1986). Reovirus guanylyl-transferase is L2 gene product lambda 2. *J. Virol.* **60,** 307–311.

Coombs, K. M. (1998). Stoichiometry of reovirus structural proteins in virus, ISVP, and core particles. *Virology* **243,** 218–228.

Drayna, D., and Fields, B. N. (1982). Activation and characterization of the reovirus transcriptase: Genetic analysis. *J. Virol.* **41,** 110–118.

Dryden, K. A., Farsetta, D. L., Wang, G., Keegan, J. M., Fields, B. N., Baker, T. S., and Nibert, M. L. (1998). Internal structures containing transcriptase-related proteins in top component particles of mammalian orthoreovirus. *Virology* **245,** 33–46.

Dryden, K. A., Wang, G., Yeager, M., Nibert, M. L., Coombs, K. M., Furlong, D. B., Fields, B. N., and Baker, T. S. (1993). Early steps in reovirus infection are associated with dramatic changes in supramolecular structure and protein conformation: Analysis of virions and subviral particles by cryoelectron microscopy and image reconstruction. *J. Cell Biol.* **122,** 1023–1041.

Esnouf, R. M. (1997). An extensively modified version of MolScript that includes greatly enhanced coloring capabilities. *J. Mol. Graphics Modelling* **15,** 132–134.

Farsetta, D. L., Chandran, K., and Nibert, M. L. (2000). Transcriptional activities of reovirus RNA polymerase in recoated cores. Initiation and elongation are regulated by separate mechanisms. *J. Biol. Chem.* **275,** 39693–39701.

Fields, B. N., Raine, C. S., and Baum, S. G. (1971). Temperature-sensitive mutants of reovirus type 3: Defects in viral maturation as studied by immunofluorescence and electron microscopy. *Virology* **43,** 569–578.

Furlong, D. B., Nibert, M. L., and Fields, B. N. (1988). Sigma 1 protein of mammalian reoviruses extends from the surfaces of viral particles. *J. Virol.* **62,** 246–256.

Furuichi, Y., LaFiandra, A., and Shatkin, A. J. (1977). 5′-Terminal structure and mRNA stability. *Nature* **266,** 235–239.

Furuichi, Y., Muthukrishnan, S., Tomasz, J., and Shatkin, A. J. (1976). Mechanism of formation of reovirus mRNA 5′-terminal blocked and methylated sequence, $^{m7}GpppG^mpC$. *J. Biol. Chem.* **251,** 5043–5053.

Harvey, J. D., Bellamy, A. R., Earnshaw, W. C., and Schutt, C. (1981).

Biophysical studies of reovirus type 3. IV. Low-angle X-ray diffraction studies. *Virology* **112,** 240–249.

Hazelton, P. R., and Coombs, K. M. (1999). The reovirus mutant tsA279 L2 gene is associated with generation of a spikeless core particle: Implications for capsid assembly. *J. Virol.* **73,** 2298–2308.

Jané-Valbuena, J., Nibert, M. L., Spencer, S. M., Walker, S. B., Baker, T. S., Chen, Y., Centonze, V. E., and Schiff, L. A. (1999). Reovirus virion-like particles obtained by recoating infectious subvirion particles with baculovirus-expressed σ3 protein: An approach for analyzing σ3 functions during virus entry. *J. Virol.* **73,** 2963–2973.

Kjeldgaard, M., Nissen, P., Thirup, S., and Nyborg, J. (1993). The crystal structure of elongation factor EF-Tu from *Thermus aquaticus* in the GTP conformation. *Structure* **1,** 35–50.

Luongo, C. L., Contreras, C. M., Farsetta, D. L., and Nibert, M. L. (1998). Binding site for *S*-adenosyl-L-methionine in a central region of mammalian reovirus λ2 protein. Evidence for activities in mRNA cap methylation. *J. Biol. Chem.* **273,** 23773–23780.

Luongo, C. L., Dryden, K. A., Farsetta, D. L., Margraf, R. L., Severson, T. F., Olson, N. H., Fields, B. N., Baker, T. S., and Nibert, M. L. (1997). Localization of a C-terminal region of λ2 protein in reovirus cores. *J. Virol.* **71,** 8035–8040.

Luongo, C. L., Reinisch, K. M., Harrison, S. C., and Nibert, M. L. (2000). Identification of the guanylyl-transferase region and active site in reovirus mRNA capping protein λ2. *J. Biol. Chem.* **275,** 2804–2810.

Mao, Z. X., and Joklik, W. K. (1991). Isolation and enzymatic characterization of protein λ2, the reovirus guanylyltransferase. *Virology* **185,** 377–386.

Mayor, H. D., and Jordan, L. E. (1968). Preparation and properties of the internal capsid components of reovirus. *J. Gen. Virol.* **3,** 233–237.

Morgan, E. M., and Kingsbury, D. W. (1981). Reovirus enzymes that modify messenger RNA are inhibition by perturbation of the lambda proteins. *Virology* **113,** 565–572.

Morgan, E. M., and Zweerink, H. J. (1974). Reovirus morphogenesis. Corelike particles in cells infected at 39 degrees with wild-type reovirus and temperature-sensitive mutants of groups B and G. *Virology* **59,** 556–565.

Morozov, S. Y. (1989). A possible relationship of reovirus putative RNA polymerase to polymerases of positive-strand RNA viruses. *Nucleic Acids Res.* **17,** 5394.

Noble, S., and Nibert, M. L. (1997a). Characterization of an ATPase activity in reovirus cores and its genetic association with core-shell protein λ1. *J. Virol.* **71,** 2182–2191.

Noble, S., and Nibert, M. L. (1997b). Core protein μ2 is a second determinant of nucleoside triphosphatase activities by reovirus cores. *J. Virol.* **71,** 7728–7735.

Reinisch, K. M., Nibert, M. L., and Harrison, S. C. (2000). Structure of the reovirus core at 3.6 Å resolution. *Nature* **404,** 960–967.

Roner, M. R., Lin, P. N., Nepluev, I., Kong, L. J., and Joklik, W. K. (1995). Identification of signals required for the insertion of heterologous genome segments into the reovirus genome. *Proc. Natl. Acad. Sci. USA* **92,** 12362–12366.

Shatkin, A. J., Furuichi, Y., LaFiandra, A. J., and Yamakawa, M. (1983). Initiation of mRNA synthesis and 5′-terminal modification of reovirus transcripts. *In* "Double-Stranded RNA Viruses" (R. W. Compans and D. H. L. Bishop, Eds.), pp. 43–54. Elsevier, New York.

Shatkin, A. J., and Kozak, M. (1983). Biochemical aspects of reovirus transcription and translation. *In* "The *Reoviridae*" (W. K. Joklik, Ed.), pp. 79–106. Plenum, New York.

Shatkin, A. J., and Sipe, J. D. (1968). RNA polymerase activity in purified reoviruses. *Proc. Natl. Acad. Sci. USA* **61,** 1462–1469.

Smith, R. E., Zweerink, H. J., and Joklik, W. K. (1969). Polypeptide components of virions, top component and cores of reovirus type 3. *Virology* **39,** 791–810.

Spencer, S. M., Sgro, J.-Y., Dryden, K. A., Baker, T. S., and Nibert, M. L. (1997). IRIS Explorer software for radial depth cueing reovirus particles and other macromolecular structures determined by transmis-

sion cryoelectron microscopy and three-dimensional image recon-
struction. *J. Struct. Biol.* **120,** 11–21.

Starnes, M. C., and Joklik, W. K. (1993). Reovirus protein λ3 is a
poly(C)-dependent poly(G) polymerase. *Virology* **193,** 356–366.

White, C. K., and Zweerink, H. J. (1976). Studies on the structure of
reovirus cores: Selective removal of polypeptide λ2. *Virology* **70,**
171–180.

Xu, P., Miller, S. E., and Joklik, W. K. (1993). Generation of reovirus
core-like particles in cells infected with hybrid vaccinia viruses that
express genome segments L1, L2, L3, and S2. *Virology* **197,** 726–731.

Yamakawa, M., Furuichi, Y., Nakashima, K., LaFiandra, A. J., and Shat-
kin, A. J. (1981). Excess synthesis of viral mRNA 5′-terminal oligonu-
cleotides by reovirus transcriptase. *J. Biol. Chem.* **256,** 6507–6514.

Yeager, M., Weiner, S., and Coombs, K. M. (1996). Transcriptionally
active reovirus core particles visualized by electron cryo-microscopy
and image reconstruction. *Biophys. J.* **70,** A116.

Yin, P., Cheang, M., and Coombs, K. M. (1996). The M1 gene is asso-
ciated with differences in the temperature optimum of the transcrip-
tase activity in reovirus core particles. *J. Virol.* **70,** 1223–1227.

Zou, S., and Brown, E. G. (1996). Stable expression of the reovirus μ2
protein in mouse L cells complements the growth of a reovirus its
mutant with a defect in its M1 gene. *Virology* **217,** 42–48.